npj | quantum materials

Article

Published in partnership with Nanjing University

https://doi.org/10.1038/s41535-024-00721-8

Chemical versus physical pressure effects on the structure transition of bilayer nickelates

Gang Wang[1,2,9], Ningning Wang[1,2,9] ✉, Tenglong Lu[1,2,9], Stuart Calder[3], Jiaqiang Yan[4], Lifen Shi[1], Jun Hou[1,2], Liang Ma[1,5], Lili Zhang[6], Jianping Sun[1,2], Bosen Wang[1,2], Sheng Meng[1,2,7], Miao Liu[1,7,8] ✉ & Jinguang Cheng[1,2] ✉

The observation of high-T_c superconductivity (HTSC) in concomitant with pressure-induced orthorhombic-tetragonal structural transition in bilayer $La_3Ni_2O_7$ has sparked hopes of achieving HTSC by stabilizing the tetragonal phase at ambient pressure. Chemical pressure, introduced by replacing La^{3+} with smaller rare-earth R^{3+} has been considered as a potential route. However, our experimental and theoretical investigation reveals that such substitutions, despite causing lattice contraction, actually produce stronger orthorhombic distortions, requiring higher pressures for the structural transition. A linear extrapolation of P_c versus the average size of A-site cations ($\langle r_A \rangle$), yields a putative critical value of $\langle r_A \rangle_c \approx 1.23$ Å for $P_c \approx 1$ bar. The negative correlation between P_c and $\langle r_A \rangle$ indicates that replacing La^{3+} with smaller R^{3+} ions is unlikely to reduce P_c to ambient pressure. Instead, substituting La^{3+} with larger cations like Sr^{2+} or Ba^{2+} might be a feasible approach. Our results provide guidance for realizing ambient-pressure HTSC in bilayer nickelates.

The recent discovery of high-T_c superconductivity (HTSC) in pressurized $La_3Ni_2O_7$ stands out as a conspicuous breakthrough in the realm of 3*d* transition-metal oxides, and has thus immediately emerged as a central subject in the community of condensed matter physics[1–30]. As a member of Ruddlesden-Popper (R-P) phase materials, $La_3Ni_2O_7$ adopts an orthorhombic *Amam* structure at ambient pressure, which consists of alternating layers of La-O and Ni-O planes with a bilayer corner-sharing $Ni^{2.5+}O_6$ octahedra structure[31–33]. Recent studies showed that it undergoes an orthorhombic to tetragonal structural transition at high pressure above $P_c \approx$ 14 GPa, which was believed to play an important role for the emergence of HTSC[1]. When the higher symmetry *I4/mmm* structure is induced by pressure, the out-of-plane Ni-O1-Ni bond angle within the bilayer corner-sharing $Ni^{2.5+}O_6$ octahedra is changed to 180°[1,6,24]. This will cause the dispersion curves originated from the $3d_{z^2}$ orbital to intersect with Fermi level, resulting in the emergency of γ band and promoting superconducting pairing[1]. Such a physical scenario was supported by subsequent theoretical calculations[9,11,12,20,34,35], and has been employed to explain the bulk superconductivity in polycrystalline $La_2PrNi_2O_7$ samples with significantly reduced intergrowth of various R-P phases[5].

As an emerging novel class of pressure-induced high-T_c superconductors, it is highly desirable to explore the possibility of achieving superconductivity at ambient pressure. One possible approach is to replace La^{3+} with either isovalent smaller-size rare-earth R^{3+} ions or heterovalent cations. While the latter affects both the lattice and charge carriers, the former solely introduces chemical pressure, which is expected to contract the lattice and reduce the physical pressure required to induce structural transition and HTSC. We are thus motivated to investigate the structural evolution of a series of rare-earth substituted $La_{3-x}R_xNi_2O_{7-\delta}$ samples under high pressure, aiming to reveal the relationship between the critical pressure P_c and the average ionic radius of the A-site cations, $\langle r_A \rangle \equiv [(3-x)\, r_{La} + x\, r_R]/3$. Considering the significant challenges in preparing single crystals of this system, we focus on the polycrystalline samples that can be prepared in a controlled manner and are conducive to sample screening before committing to dedicated crystal growth endeavor[2,5,31].

[1]Beijing National Laboratory for Condensed Matter Physics and Institute of Physics, Chinese Academy of Sciences, 100190 Beijing, China. [2]School of Physical Sciences, University of Chinese Academy of Sciences, 100190 Beijing, China. [3]Neutron Scattering Division, Oak Ridge National Laboratory, Oak Ridge, TN, 37831, USA. [4]Materials Science and Technology Division, Oak Ridge National Laboratory, Oak Ridge, TN, 37831, USA. [5]Key Laboratory of Materials Physics, Ministry of Education, School of Physics and Microelectronics, Zhengzhou University, Zhengzhou, 450052, China. [6]Shanghai Synchrotron Radiation Facility, Shanghai Advanced Research Institute, Chinese Academy of Sciences, Shanghai, 201204, China. [7]Songshan Lake Materials Laboratory, Dongguan, 523808, China. [8]Center of Materials Science and Optoelectronics Engineering, University of Chinese Academy of Sciences, 100049 Beijing, China. [9]These authors contributed equally: Gang Wang, Ningning Wang, Tenglong Lu. ✉e-mail: nnwang@iphy.ac.cn; mliu@iphy.ac.cn; jgcheng@iphy.ac.cn

In this work, we prepared a series of $La_{3-x}R_xNi_2O_{7-\delta}$ (R = Pr, Nd, Tb, Y) polycrystalline samples with the same procedures and conducted systematic high-pressure (HP) synchrotron X-ray diffraction (SXRD) to determine the critical pressure P_c for the structural transition. The constructed phase diagram of P_c versus $\langle r_A \rangle$ reveals that P_c rises monotonically with the reduction of $\langle r_A \rangle$, which is attributed to the enhanced orthorhombic distortion upon reducing $\langle r_A \rangle$. This observation indicates that it is unlikely to reduce P_c through the substitution of smaller R^{3+} at the La position. In addition, the extrapolation of P_c versus $\langle r_A \rangle$ suggests that it is likely to reduce P_c to ambient pressure via substituting La^{3+} with larger heterovalent cations, such as alkaline-earth Sr^{2+} or Ba^{2+}. By unveiling a negative relationship between P_c and $\langle r_A \rangle$, our results provide valuable insights in achieving superconductivity at ambient pressure in this system.

Results

Impact of chemical pressure

The phase purity of obtained $La_{3-x}R_xNi_2O_{7-\delta}$ samples was first examined with XRD at room temperature. As shown in Fig. S1, all samples are confirmed to be single phase with the orthorhombic *Amam* structure (No. 63). The substitution of smaller R^{3+} for La^{3+} in the perovskite-type $La_3Ni_2O_7$ is expected to shrink the lattice and enhance local structural distortions. To obtain reliable information about the structural changes upon different R^{3+} substitutions, we performed NPD measurements at ambient conditions since the oxygen atoms have a large neutron scattering length. Figure 1a and Table S1 display the Rietveld refinement results on the collected NPD data, which further confirm that all samples are single phase with the orthorhombic structure. The obtained lattice parameters are displayed in Fig. 1b, c as a function of $\langle r_A \rangle$. As can be seen, the lattice parameters exhibit anisotropic shrinkage with increasing $\langle r_A \rangle$, i.e., a and c are reduced monotonically by 0.6% and 0.9%, respectively, while b remains nearly unchanged, resulting in a net volume reduction of 1.5% from $La_3Ni_2O_{7-\delta}$ to $La_{1.8}Nd_{1.2}Ni_2O_{7-\delta}$. Such an evolution confirms that we have successfully introduced some chemical pressure into the $La_3Ni_2O_7$ lattice by replacing La^{3+} with smaller R^{3+}.

The observed anisotropic evolutions of in-plane lattice parameters motivated us to inspect the local structure arrangements of the buckled NiO_2 planes in the orthorhombic bilayer nickelates. As shown in Fig. S2a, the lattice parameters a and $b \approx 2\sqrt{2}$ (Ni-O) are determined by a combination of Ni-O bond lengths, Ni-O-Ni and O-Ni-O bond angles. Since both Ni-O3/Ni-O4 bond lengths and Ni-O3/O4-Ni bond angles with similar magnitudes are involved in determining the a and b axes, their relative magnitudes are mainly determined by the O-Ni-O angles as illustrated in Fig. S2a. It is the obtuse angle O3-Ni-O4 and the acute angles of O3-Ni-O3 and O4-Ni-O4 that results in the experimentally observed $b > a$. As shown in Fig. S2b, upon reducing $\langle r_A \rangle$, the obtuse angle O3-Ni-O4 is monotonically enlarged while the average of acute angles O3-Ni-O3 and O4-Ni-O4 is slightly reduced. These factors alone should result in a monotonic elongation of b and shortening of a. Considering the general reduction trends of in-plane bond lengths and angles that should reduce both a and b, the above-mentioned elongation trend of b will be partially compensated while the declining trend of a be further enhanced, resulting in anisotropic variations of a and b as a function of $\langle r_A \rangle$ shown in Fig. 1b.

Although the chemical and physical pressures play similar roles in shrinking the overall lattice, their influences on the local structural distortions are distinct. For example, external physical pressure usually compresses the lattice uniformly and drives it to a higher symmetry, while the chemical pressure produces stronger local structural distortions in the perovskite-type structures. As shown in Fig. 1d, e, some interesting features about the local structural modifications induced by smaller R^{3+} are noteworthy: (1) both the out-of-plane Ni-O2/O1 bonds first experience an elongation, reaching the maximum at $\langle r_A \rangle$ = 1.206 Å, and then decreases upon further reducing $\langle r_A \rangle$ for $La_{1.8}Nd_{1.2}Ni_2O_7$; (2) the in-plane Ni-O3 and Ni-O4 bond lengths vary oppositely, resulting in reduction first and then an enhanced splitting of in-plane Ni-O bonds as a function of $\langle r_A \rangle$; (3) both in-plane and out-of-plane buckling of the corner-shared NiO_6 octahedra becomes stronger as the Ni-O-Ni bond angles are reduced. Based on the limited data points in Fig. 1d, e, there seems to exist an anomalous trend for $La_{1.8}Nd_{1.2}Ni_2O_{7-\delta}$. However, the presence of four distinct Ni-O bond lengths and three Ni-O-Ni bond angles makes it quite complicated to characterize the overall orthorhombic distortions associated with the tilting and bulking of NiO_6 octahedra. To a first-order approximation, here we examine the variations of average <Ni-O> bond length and <Ni-O-Ni> bond angle as a function of $\langle r_A \rangle$. As shown in Fig. S3, the average <Ni-O>

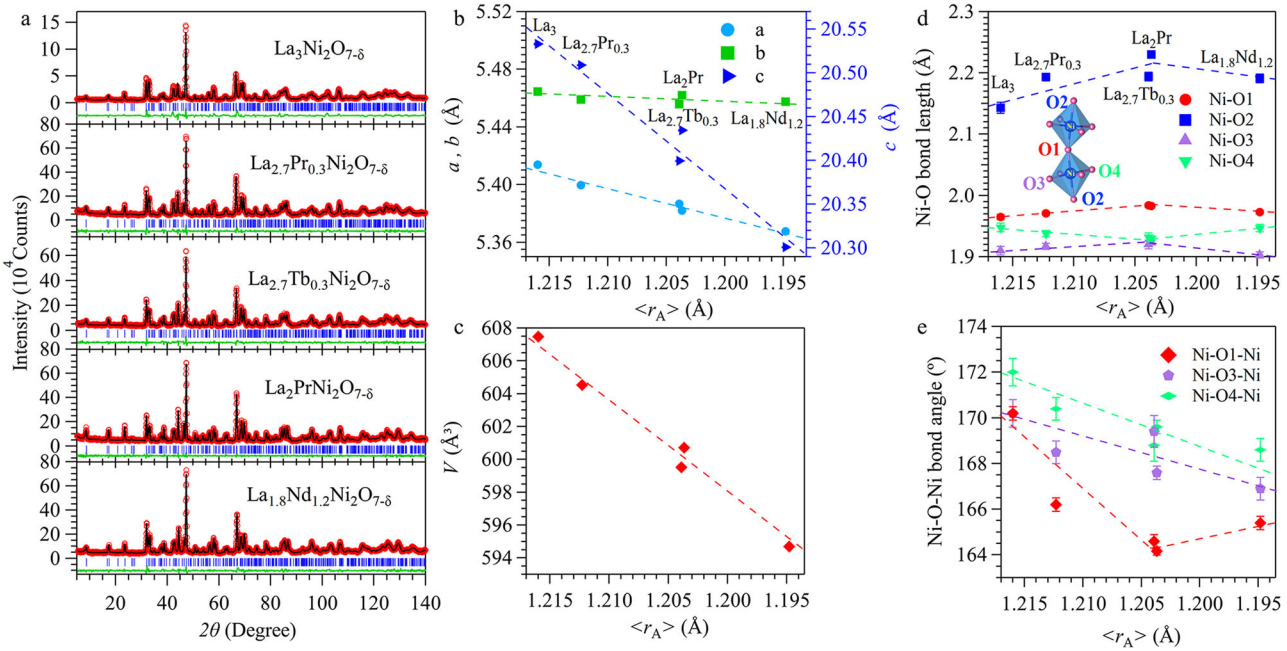

Fig. 1 | Structural characterizations of the $La_{3-x}R_xNi_2O_{7-\delta}$ (R = Pr, Nd, Tb) polycrystalline samples. a Rietveld refinements on the NPD data with the space group *Amam*. **b–e** The obtained lattice parameters, unit-cell volume, Ni-O bond lengths and Ni-O-Ni bond angles as a function of the average ionic radius of the *A*-site cations, $\langle r_A \rangle$, across the series of $La_{3-x}R_xNi_2O_{7-\delta}$ (R = Pr, Nd, Tb) polycrystalline samples. The NPD data for $La_{3-x}Pr_xNi_2O_{7-\delta}$ (x = 0, 1.0) samples were adopted from our previous study[2,5]. The error bars in (**b–d**) are smaller than symbols.

bond length keeps nearly constant around 1.98 ± 0.01 Å, while the average <Ni-O-Ni> bond angle decreases linearly with reducing $<r_A>$. Therefore, the substitutions of smaller R^{3+} for La^{3+} in $La_{3-x}R_xNi_2O_{7-\delta}$ not only shrink the overall lattice but also produce stronger local orthorhombic distortions. The former effect is similar as external physical pressure, whereas the latter one should require higher pressure to induce a structural transition to a higher symmetry.

Pressure-induced structural transition of $La_{3-x}R_xNi_2O_{7-\delta}$

To determine the critical pressure P_c for structural transition, we conducted HP-SXRD measurements at room temperature under various pressures up to 40 GPa. The HP-SXRD results on two representative samples, $La_3Ni_2O_{7-\delta}$ and $La_{1.8}Nd_{1.2}Ni_2O_{7-\delta}$, are depicted in Fig. 2a, b, respectively. For $La_3Ni_2O_{7-\delta}$, the SXRD patterns below 4.9 GPa consistently match the orthorhombic *Amam* structure, as shown by the representative refinement at 3.6 GPa (Fig. 2c). However, upon compression to 7.0 GPa, several adjacent peaks merge, such as the (020) and (200) peaks at ~13.4°, as illustrated in the right panel of Fig. 2a. This observation suggests the occurrence of pressure-induced structural transition towards higher symmetry. Subsequent structure analyses revealed that the SXRD patterns of the HP phase can be better described using the $Sr_3Ti_2O_7$-type structural model with the tetragonal *I4/mmm* space group (No. 139), Fig. 2d, consistent with previously reported results[24]. For $La_{1.8}Nd_{1.2}Ni_2O_{7-\delta}$, the same structural transition was also observed, with the critical pressure $P_c \approx 17$ GPa (Fig. 2b, e, f). The HP-SXRD results for the other three samples of the $La_{3-x}R_xNi_2O_{7-\delta}$ (R = Pr, Tb, Y) series were shown in Figs. S4–S6. They all undergo the same structural phase transition under high pressure with the $P_c \approx 8$, 10.5, and 8.7 GPa for $La_{2.7}Pr_{0.3}Ni_2O_{7-\delta}$, $La_{2.7}Tb_{0.3}Ni_2O_{7-\delta}$, and $La_{2.87}Y_{0.13}Ni_2O_{7-\delta}$, respectively.

Figure 3 displays the lattice parameters as a function of pressure for these two samples extracted from their HP-SXRD patterns after Rietveld refinements. As seen from Fig. 3a, b, their lattice parameters decrease continuously with increasing pressure, but exhibit anisotropic compressions. In the lower pressure range, lattice parameter b decreases faster than a and they converge at P_c, where the structural transition takes place. As the crystal structure transforms into a higher-symmetry tetragonal structure, the lattice parameter a contracts by a factor of $\frac{1}{\sqrt{2}}$, leading to a 0.5 times reduction in the unit-cell volume, V. The collected pressure-volume $P(V)$ data in the whole pressure range can be fitted to the third-order Birch-Murnaghan equation[36], yielding a bulk modulus of $B_0^{orth} = 137.1$ GPa and $B_0^{tetra} = 208.4$ GPa for $La_3Ni_2O_{7-\delta}$ and $B_0^{orth} = 179.3$ GPa and $B_0^{tetra} = 221.7$ GPa for $La_{1.8}Nd_{1.2}Ni_2O_{7-\delta}$, respectively, with B_0' fixed at 3.5, as shown by the dashed lines in Fig. 3c, d.

DFT insights on structural transition

From the above experimental results, we can see that P_c increases with reducing $<r_A>$. To understand the structural transition of bilayer nickelates as a function of chemical and physical pressures, we employed the DFT calculations to study the structural evolution of the $R_3Ni_2O_{7-\delta}$ (R = La, Pr, Nd) samples under high pressure. Figure 4 shows the calculated results of lattice parameters for $R_3Ni_2O_{7-\delta}$ (R = La, Pr, Nd) as a function of external pressure. As can be seen, all $R_3Ni_2O_7$ compounds undergo an orthorhombic to tetragonal structural transition under high pressure, consistent with the experimental observations mentioned above. Additionally, our DFT calculations show that the calculated P_c at $U = 3$ eV for $La_3Ni_2O_7$ is ~9 GPa, which is close to the HP-SXRD observations, indicating the reliability and accuracy of our theoretical methods. It should be noted that the critical

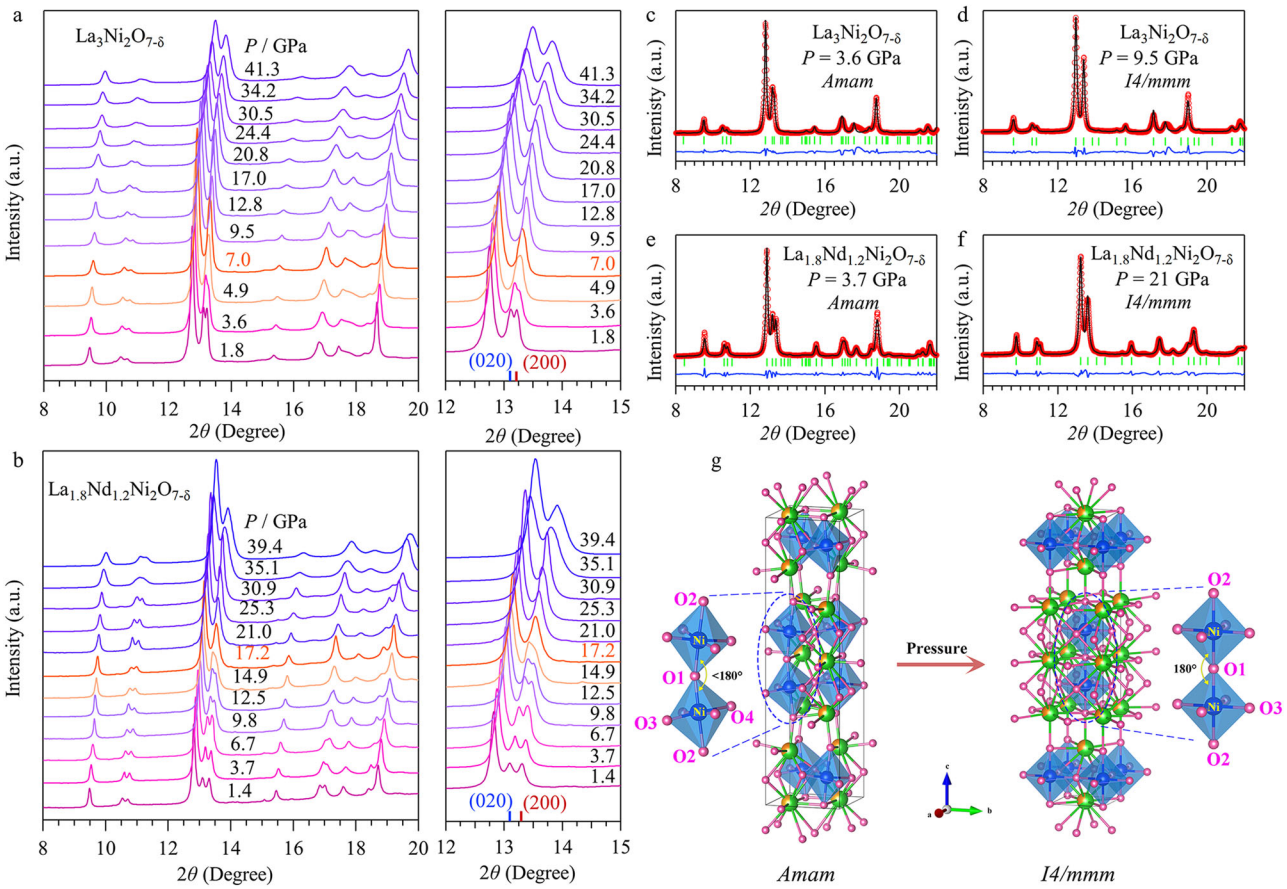

Fig. 2 | Pressure-induced structural transition. a, **b** SXRD patterns of $La_3Ni_2O_{7-\delta}$ and $La_{1.8}Nd_{1.2}Ni_2O_{7-\delta}$ polycrystalline samples under various pressures up to 41.3 and 39.4 GPa, respectively. The enlarged view of SXRD around the representative 2θ ranges highlight the gradual merging of the diffraction peaks upon compression. **c**–**f** Refinement results of the SXRD patterns at pressures before and after the structural phase transition for $La_3Ni_2O_{7-\delta}$ and $La_{1.8}Nd_{1.2}Ni_2O_{7-\delta}$. **g** Crystal structure transformation of $La_{3-x}R_xNi_2O_{7-\delta}$ under high pressure.

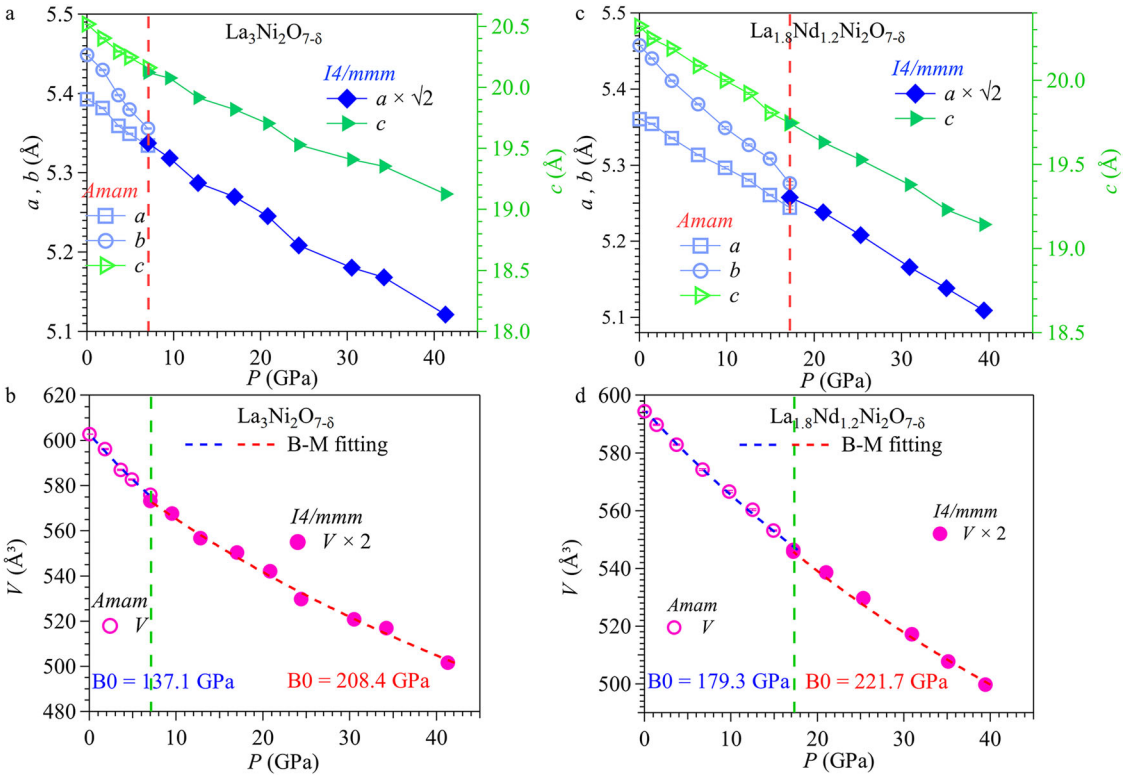

Fig. 3 | The evolution of lattice parameters under high pressure for $La_3Ni_2O_{7-\delta}$ and $La_{1.8}Nd_{1.2}Ni_2O_{7-\delta}$ polycrystalline samples. Lattice parameters and cell volume as a function of pressure for **a**, **b** $La_3Ni_2O_{7-\delta}$ and **c**, **d** $La_{1.8}Nd_{1.2}Ni_2O_{7-\delta}$ samples under various pressures up to 41.3 and 39.4 GPa, respectively. The critical pressure P_c for the structural transition is marked by the vertical broken line in (**b**, **d**).

pressure P_c from DFT calculations depends sensitively on the choice of Hubbard U values, and a higher U value results in a lower calculated P_c. As shown in Fig. S7, the calculated P_c of $La_3Ni_2O_7$ decreases monotonically from ~ 12 GPa for $U = 1$ eV to ~ 5 GPa for $U = 6$ eV. The U value of 3 eV applied in this work is favored by many theoretical studies of this system[7,9,15,19,37] and is close to the value of ~3.5 eV obtained from angle-resolved photoelectron spectroscopy experiments[21].

To better clarify the impact of physical pressure on the structural evolution of the system, we extracted the bond lengths and bond angles of $La_3Ni_2O_7$ under various pressures from DFT calculations. As shown in Fig. S8a, all bond lengths decrease progressively with applied pressure but exhibit anisotropic compressions. For the two out-of-plane bonds, Ni-O2 shortens more rapidly than Ni-O1 with increasing pressure, leading to a reduction in the length difference between these bonds. For the in-plane bonds, Ni-O4 decreases in length faster than Ni-O3, and they converge at the critical pressure P_c. In addition, as the Ni–O–Ni bond angle gradually increases with pressure and reaches 180° at P_c, both in-plane and out-of-plane buckling of the corner-shared NiO_6 octahedra are diminished (Fig. S8b). It is noteworthy that these calculated changes of bond lengths and angles under physical pressure are different from those induced by reducing $\langle r_A \rangle$ shown in Fig. 1b, d, e, further highlighting the distinct effects of physical pressure versus chemical pressure on the structural evolution as discussed above.

P_c -$\langle r_A \rangle$ phase diagram

We plotted in Fig. 5 the obtained P_c of $La_{3-x}R_xNi_2O_{7-\delta}$ from both experiments and DFT calculations as a function of $\langle r_A \rangle$. As seen clearly, P_c increases with the reduction of $\langle r_A \rangle$. This result reveals that the structural transition is dictated mainly by the local orthorhombic distortions in chemically pre-compressed $La_{3-x}R_xNi_2O_{7-\delta}$ samples, i.e., the stronger local structural distortion, the higher P_c for structural transition. The observed evolution of P_c versus $\langle r_A \rangle$ implies that it is not feasible to reduce P_c to ambient pressure via substituting La^{3+} with smaller-size R^{3+} ions. A linear extrapolation of P_c versus $\langle r_A \rangle$ to zero would yield an $\langle r_A \rangle_c \approx 1.232$ Å for the stabilization of the tetragonal phase at ambient pressure, as shown by the black dashed line in Fig. 5. If this assumption holds, alkaline-earth-metal substituted $La_{2.5}Sr_{0.5}Ni_2O_7$ and $La_{2.8}Ba_{0.2}Ni_2O_7$ can satisfy such a requirement of $\langle r_A \rangle \approx 1.232$ Å. In addition, extra charge carriers will be introduced into this system by doping alkaline-earth cations. Although the replacement of La^{3+} with heterovalent alkaline-earth cations could be a viable approach to stabilize the tetragonal phase at ambient pressure, it remains quite challenging to synthesize these samples.

Discussion

Recently, Jiao et al.[18] synthesized a series of Sr-doped $La_{3-x}Sr_xNi_2O_{7-\delta}$ ($0 \le x \le 0.1$) polycrystalline samples via conventional solid-state-reaction method. They found that upon increasing x, the lattice constants a and b expand while the c-axis contracts, with a simultaneous increase of Ni-O-Ni bond angles. In addition, the resistivity decreases monotonically in the entire temperature range due to the introduction of hole carriers and the reduced structural distortions. Xu et al.[38] successfully obtained Sr-doped $La_{2.8}Sr_{0.2}Ni_2O_{6.95}$ single crystals with the orthorhombic bilayer structure by treating the precursors at 20 GPa and 1400 °C in a Walker-type multi-anvil press. For such samples, both out-of-plane Ni–O–Ni bond angles of 173.4(2)° and in-plane Ni-O-Ni bond angles of 175.0(2)° and 176.7(2)° are indeed larger than those of pristine $La_3Ni_2O_7$. The HP-SXRD was not performed on those $La_{3-x}Sr_xNi_2O_{7-\delta}$ polycrystalline samples and $La_{2.8}Sr_{0.2}Ni_2O_{6.95}$ single crystal. According to the present study, it is expected that the structural transition to the tetragonal phase should take place at a lower P_c than $La_3Ni_2O_7$. Thus, HP structural studies on these samples are highly desirable. Intriguingly, it was found that the $La_{2.8}Sr_{0.2}Ni_2O_{6.95}$ single crystal exhibits an insulating behavior at ambient pressure and displays pressure-driven insulator-metal-insulator crossovers up to 19 GPa. These transport properties are dramatically different from

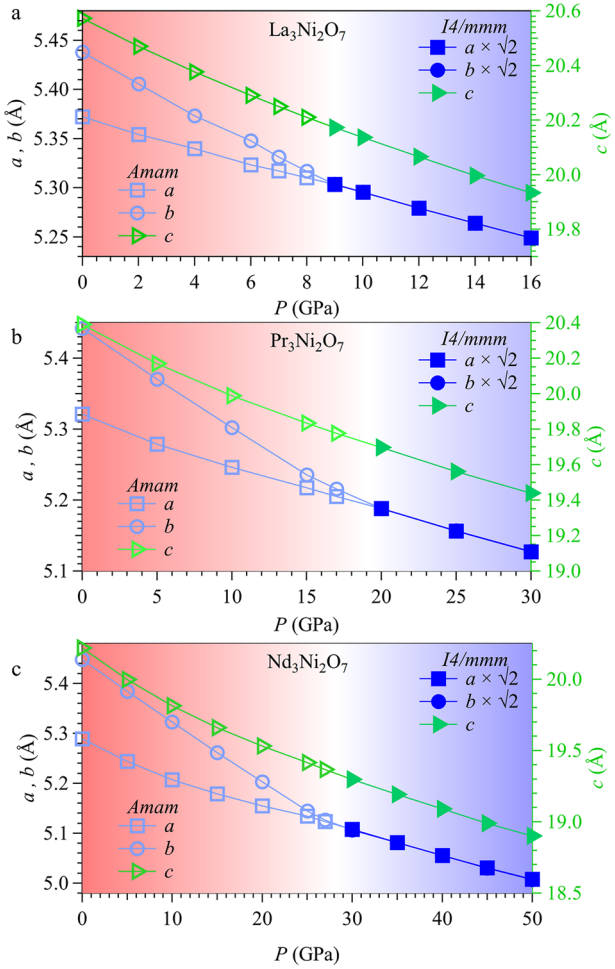

Fig. 4 | The calculated structural evolutions as a function of pressure. a–c Lattice parameters of $R_3Ni_2O_7$ (R = La, Pr, Nd) as a function of the external pressure from DFT calculations. As can be seen, the lattice parameters a and b of all $R_3Ni_2O_7$ compounds gradually converge under high pressure, but with different critical pressures.

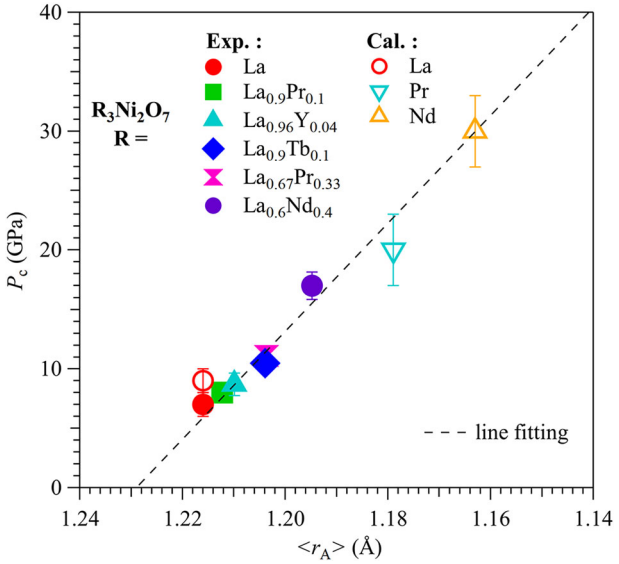

Fig. 5 | The constructed P_c -$<r_A>$ phase diagram. The critical pressure P_c for the orthorhombic-tetragonal structural transition as a function of the average ionic radius of the A-site cations, $<r_A>$, across the series of $La_{3-x}R_xNi_2O_{7-\delta}$ (R = Pr, Nd, Tb, Y) polycrystalline samples. As can be seen, the data derived from theoretical calculations and experiments can be well described by linear fitting. The error bars are mainly determined by the pressure intervals in either SXRD experiments or theoretical calculations.

those of the parent compound $La_3Ni_2O_{7-\delta}$ and warrant further investigation. Nevertheless, the successful synthesis of Sr-doped $La_{2.8}Sr_{0.2}Ni_2O_{6.95}$ single crystals would open an avenue for exploring possible ambient-pressure HTSC via further enhancing the substitution levels of Sr^{2+} for La^{3+} in the bilayer nickelates.

It is noteworthy that the critical pressure $P_c \approx 7$ GPa for our polycrystalline $La_3Ni_2O_{7-\delta}$ sample is lower than that of ~14 GPa for the single-crystal samples reported by Sun et al. in ref. 1. At present, the origin of this discrepancy remains unclear, which might arise from the distinct grain sizes or diverse levels of structure defects/disorders for the different forms of samples. Nonetheless, our HP-SXRD results on the polycrystalline $La_{3-x}R_xNi_2O_{7-\delta}$ samples prepared at the same conditions should provide self-consistent information about the effect of substitution of smaller R^{3+} ions at the La sites.

Based on our combined HP-SXRD and resistivity measurements on the polycrystalline $La_{3-x}Pr_xNi_2O_{7-\delta}$ (x = 0 and 1) samples, we found that the emergence of superconductivity is in general concomitant with the structural transition in this system. For the $La_3Ni_2O_{7-\delta}$ sample, the structural transition occurs at $P_c \approx 7$ GPa, while the resistance begins to decrease around 6–8 GPa and reaches zero at roughly 9 GPa[2]. Similarly, the structure transition takes place at $P_c \approx 11$ GPa while the resistance drop appears at ~ 8 GPa and approaches zero at about 11 GPa for $La_2PrNi_2O_7$[5]. Some discrepancies between the critical pressures for structural transition and the emergence of superconductivity should be partially ascribed to the pressure distribution/variation in different HP techniques. This effect should be magnified for the pressure cells upon cooling down. It is noted that the structural transition was monitored via HP-SXRD measurements at room temperature whereas the emergence of superconductivity was evidenced by HP-resistance measurements at low temperatures. We have shown in our previous study that the pressure values in palm-type cubic anvil cell (CAC) for resistance measurements will change upon cooling down due to the thermal contraction mismatch of different parts of pressure cells[39]. For example, the CAC locked at 8 GPa at room temperature increases to ~10.5 GPa at low temperatures. Considering these extrinsic factors, the critical pressures for the orthorhombic-tetragonal structural transition are in general coincidence with the emergence of superconductivity in the bilayer nickelates.

The series of $La_{3-x}R_xNi_2O_{7-\delta}$ samples prepared in the present study offer an excellent material platform for comprehensive investigations on structure-property correlations. As the $P_c \approx 17$ GPa of $La_{1.8}Nd_{1.2}Ni_2O_{7-\delta}$ is over the pressure limit of our CAC apparatus and is also close to the limit of two-stage multianvil pressure cell, we have to employ the diamond anvil cell (DAC) to measure its HP resistance. Some preliminary results (not shown here) indeed evidenced the onset of superconductivity at an elevated pressure ~16 GPa, further reinforcing the intimated correlation between structural transition and the emergence of superconductivity in these bilayer nickelates. However, due to the non-hydrostatic pressure conditions in DAC filled with solid pressure transmitting medium, we can only observe the drop of resistance without reaching zero resistance. For these bilayer nickelates, it is highly desirable for resistance measurements under hydrostatic pressures above 20 GPa.

Finally, we would like to highlight that the experimentally observed P_c for structural transition can be excellently simulated by DFT calculations, which demonstrated the power and accuracy of structural modeling using ab initio calculations. Thus, incorporating simulations into future research may provide valuable insights before conducting specific experiments. This can potentially accelerate material discovery and lead to more favorable outcomes while reducing experimental workload.

In summary, we conducted systematic HP-SXRD measurements on a series of $La_{3-x}R_xNi_2O_{7-\delta}$ (R = Pr, Nd, Tb, Y) samples and established a

quantitative relationship between the critical pressure P_c for orthorhombic-tetragonal structural transition and the average size of A-site cations, $\langle r_A \rangle$. By unveiling the inverse relationship between P_c and $\langle r_A \rangle$, our results provide useful guidelines for achieving the tetragonal phase at ambient pressure in this system. Replacing La with alkaline-earth metals can increase $\langle r_A \rangle$ and introduce additional charge carriers, making it a promising approach to achieve HTSC at ambient pressure.

Methods

Sample synthesis

A series of $La_{3-x}R_xNi_2O_{7-\delta}$ (R = Pr, Nd, Tb, Y) polycrystalline samples were synthesized by the sol-gel method as described in refs. 2,31. Stoichiometric mixtures of rare-earth oxides and $Ni(NO_3)_2{\cdot}6H_2O$ (99.99%, Alfa Aesar) were used as the starting materials. All samples were synthesized using the identical procedures and sintered at the same temperature conditions. Each dopant has its own solubility, which we determined by experimenting with different compositions. In this work, the highest experimentally obtained doping level of $La_{3-x}R_xNi_2O_{7-\delta}$ (R = Pr, Nd, Tb, Y) samples with a pure phase are $La_2PrNi_2O_{7-\delta}$, $La_{1.8}Nd_{1.2}Ni_2O_{7-\delta}$, $La_{2.7}Tb_{0.3}Ni_2O_{7-\delta}$, and $La_{2.87}Y_{0.13}Ni_2O_{7-\delta}$. Further increasing the substitution content results in the formation of (La, R)$_2$NiO$_4$ or other oxide impurities.

Structural characterizations

The phase purity and crystal structure of $La_{3-x}R_xNi_2O_{7-\delta}$ at ambient conditions were determined by powder X-ray diffraction (XRD) collected via a Huber diffractometer with Cu-K_α radiation. Neutron powder diffraction (NPD) measurements were carried out using the HB-2A diffractometer at the High Flux Isotope Reactor (HFIR) of Oak Ridge National Laboratory (ORNL)[40,41]. Powder samples of $La_{3-x}R_xNi_2O_{7-\delta}$ were placed inside a 6 mm-diameter vanadium container and then inserted into a closed cycle refrigerator. NPD data was collected at 295 K, utilizing a constant wavelength of λ = 1.5365 Å, derived from the Ge (115) monochromator. The NPD pattern was collected by scanning a 120° bank of 44 ^{3}He detectors in 0.05° steps to give 2θ coverage from 5° to 150°. Rietveld refinements were performed with the FULLPROF program[42]. HP-SXRD measurements were performed at BL15U1 station of Shanghai Synchrotron Radiation Facility (SSRF) with a wavelength of λ = 0.6199 Å. Rietveld analysis was performed with GSAS-II program[43].

DFT structure calculations

Density functional theory (DFT) calculations were conducted using the projector-augmented wave (PAW) method, implemented in the Vienna ab initio simulation package (VASP)[44,45]. All calculations utilized the Perdew-Burke-Ernzerhof (PBE) generalized gradient approximation (GGA) exchange-correlation functional[46]. To correct the self-interaction error on the Ni species, a rotationally averaged Hubbard U correction of 3 eV was applied[47]. This value is commonly used in theoretical studies of this system[7,9,15,19,37] and is close to the value of ~3.5 eV obtained from the angle-resolved photoelectron spectroscopy experiments[21]. For all calculations, a plane wave energy cutoff of 520 eV, an electronic minimization threshold of 10^{-6} eV, and a k-point grid of $n_{kpoints} \times n_{atoms} > 1000$ were adopted. For structural relaxation, all degrees of freedom of atoms and lattices were allowed to relax until the atomic forces were less than 0.001 eV Å^{-1}. Given that $La_3Ni_2O_7$ displays no long-range magnetic ordering in previous experiments[1], all DFT calculations in this study were performed without spin-polarization. The PSTRESS parameter was employed to control the external hydrostatic pressure.

Data availability

The data that support the findings of this study are available from the corresponding author upon reasonable request.

Received: 5 September 2024; Accepted: 18 December 2024;
Published online: 02 January 2025

References

1. Sun, H. et al. Signatures of superconductivity near 80 K in a nickelate under high pressure. *Nature* **621**, 493–498 (2023).
2. Wang, G. et al. Pressure-induced superconductivity in polycrystalline $La_3Ni_2O_{7-\delta}$. *Phys. Rev. X* **14**, 011040 (2024).
3. Zhang, Y. et al. High-temperature superconductivity with zero resistance and strange-metal behaviour in $La_3Ni_2O_{7-\delta}$. *Nat. Phys.* **20**, 1269–1273 (2024).
4. Hou, J. et al. Emergence of high-temperature superconducting phase in the pressurized $La_3Ni_2O_7$ crystals. *Chin. Phys. Lett.* **40**, 117302 (2023).
5. Wang, N. et al. Bulk high-temperature superconductivity in pressurized tetragonal $La_2PrNi_2O_7$. *Nature* **634**, 579–584 (2024).
6. Wang, M., Wen, H.-H., Wu, T., Yao, D.-X. & Xiang, T. Normal and superconducting properties of $La_3Ni_2O_7$. *Chin. Phys. Lett.* **41**, 077402 (2024).
7. Sakakibara, H., Kitamine, N., Ochi, M. & Kuroki, K. Possible high T_c superconductivity in $La_3Ni_2O_7$ under high pressure through manifestation of a nearly half-filled bilayer hubbard model. *Phys. Rev. Lett.* **132**, 106002 (2024).
8. Qu, X.-Z. et al. Bilayer $t-J-J_\perp$ model and magnetically mediated pairing in the pressurized nickelate $La_3Ni_2O_7$. *Phys. Rev. Lett.* **132**, 036502 (2024).
9. Luo, Z., Hu, X., Wang, M., Wú, W. & Yao, D.-X. Bilayer two-orbital model of $La_3Ni_2O_7$ under pressure. *Phys. Rev. Lett.* **131**, 126001 (2023).
10. Lu, C., Pan, Z., Yang, F. & Wu, C. Interlayer-coupling-driven high-temperature superconductivity in $La_3Ni_2O_7$ under pressure. *Phys. Rev. Lett.* **132**, 146002 (2024).
11. Liu, Y.-B., Mei, J.-W., Ye, F., Chen, W.-Q. & Yang, F. s$^\pm$-wave pairing and the destructive role of apical-oxygen deficiencies in $La_3Ni_2O_7$ under pressure. *Phys. Rev. Lett.* **131**, 236002 (2023).
12. Jiang, R., Hou, J., Fan, Z., Lang, Z.-J. & Ku, W. Pressure driven fractionalization of ionic spins results in cupratelike high-T_c superconductivity in $La_3Ni_2O_7$. *Phys. Rev. Lett.* **132**, 126503 (2024).
13. Christiansson, V., Petocchi, F. & Werner, P. Correlated electronic structure of $La_3Ni_2O_7$ under pressure. *Phys. Rev. Lett.* **131**, 206501 (2023).
14. Chen, K. et al. Evidence of spin density waves in $La_3Ni_2O_{7-\delta}$. *Phys. Rev. Lett.* **132**, 256503 (2024).
15. Rhodes, L. C. & Wahl, P. Structural routes to stabilize superconducting $La_3Ni_2O_7$ at ambient pressure. *Phys. Rev. Mater.* **8**, 044801 (2024).
16. Li, F. et al. Design and synthesis of three-dimensional hybrid Ruddlesden-Popper nickelate single crystals. *Phys. Rev. Mater.* **8**, 053401 (2024).
17. Wú, W., Luo, Z., Yao, D.-X. & Wang, M. Superexchange and charge transfer in the nickelate superconductor $La_3Ni_2O_7$ under pressure. *Sci. China Phys. Mech. Astron.* **67**, 117402 (2024).
18. Jiao, K. et al. Enhanced conductivity in Sr doped $La_3Ni_2O_{7-\delta}$ with high-pressure oxygen annealing. *Phys. C Supercond. Appl.* **621**, 1354504 (2024).
19. Geisler, B., Hamlin, J. J., Stewart, G. R., Hennig, R. G. & Hirschfeld, P. J. Structural transitions, octahedral rotations, and electronic properties of $A_3Ni_2O_7$ rare-earth nickelates under high pressure. *npj Quantum Mater.* **9**, 38 (2024).
20. Zhang, Y., Lin, L. F., Moreo, A., Maier, T. A. & Dagotto, E. Structural phase transition, s$^\pm$-wave pairing, and magnetic stripe order in bilayered superconductor $La_3Ni_2O_7$ under pressure. *Nat. Commun.* **15**, 2470 (2024).
21. Yang, J. et al. Orbital-dependent electron correlation in double-layer nickelate $La_3Ni_2O_7$. *Nat. Commun.* **15**, 4373 (2024).
22. Dong, Z. et al. Visualization of oxygen vacancies and self-doped ligand holes in $La_3Ni_2O_{7-\delta}$. *Nature* **630**, 847–852 (2024).
23. Kakoi, M. et al. Multiband metallic ground state in multilayered nickelates $La_3Ni_2O_7$ and $La_4Ni_3O_{10}$ probed by ^{139}La-NMR at ambient pressure. *J. Phys. Soc. Jpn.* **93**, 053702 (2024).

24. Wang, L. et al. Structure responsible for the superconducting state in $La_3Ni_2O_7$ at high-pressure and low-temperature conditions. *J. Am. Chem. Soc.* **146**, 7506–7514 (2024).
25. Chen, X. et al. Polymorphism in the Ruddlesden–Popper nickelate $La_3Ni_2O_7$: discovery of a hidden phase with distinctive layer stacking. *J. Am. Chem. Soc.* **146**, 3640–3645 (2024).
26. Wang, H., Chen, L., Rutherford, A., Zhou, H. & Xie, W. Long-range structural order in a hidden phase of Ruddlesden-Popper bilayer nickelate $La_3Ni_2O_7$. *Inorg. Chem.* **63**, 5020–5026 (2024).
27. Shen, Y., Qin, M. & Zhang, G.-M. Effective bi-Layer model hamiltonian and density-matrix renormalization group study for the High-T_c superconductivity in $La_3Ni_2O_7$ under high pressure. *Chin. Phys. Lett.* **40**, 127401 (2023).
28. Jiang, K., Wang, Z. & Zhang, F.-C. High-temperature superconductivity in $La_3Ni_2O_7$. *Chin. Phys. Lett.* **41**, 017402 (2024).
29. Ouyang, Z., Gao, M. & Lu, Z.-Y. Absence of electron-phonon coupling superconductivity in the bilayer phase of $La_3Ni_2O_7$ under pressure. *npj Quantum Mater.* **9**, 80 (2024).
30. Luo, Z., Lv, B., Wang, M., Wú, W. & Yao, D.-X. High-TC superconductivity in $La_3Ni_2O_7$ based on the bilayer two-orbital *t-J* model. *npj Quantum Mater.* **9**, 61 (2024).
31. Zhang, Z., Greenblatt, M. & Goodenough, J. B. Synthesis, structure, and properties of the layered perovskite $La_3Ni_2O_{7-\delta}$. *J. Solid State Chem.* **108**, 402–409 (1994).
32. Greenblatt, M. Ruddlesden-Popper $Ln_{n+1}Ni_nO_{3n+1}$ nickelates: structure and properties. *Curr. Opin. Solid State Mater. Sci.* **2**, 174–183 (1997).
33. Ling, C. D., Argyriou, D. N., Wu, G. & Neumeier, J. J. Neutron diffraction study of $La_3Ni_2O_7$: structural relationships among n=1, 2, and 3 phases $La_{n+1}Ni_nO_{3n+1}$. *J. Solid State Chem.* **152**, 517–525 (2000).
34. Yang, Y.-f, Zhang, G.-M. & Zhang, F.-C. Interlayer valence bonds and two-component theory for high-T_c superconductivity of $La_3Ni_2O_7$ under pressure. *Phys. Rev. B.* **108**, L201108 (2023).
35. Zhang, Y., Lin, L.-F., Moreo, A., Maier, T. A. & Dagotto, E. Electronic structure, magnetic correlations, and superconducting pairing in the reduced Ruddlesden-Popper bilayer $La_3Ni_2O_6$ under pressure: different role of d_{3z^2-r2} orbital compared with $La_3Ni_2O_7$. *Phys. Rev. B.* **109**, 045151 (2024).
36. Birch, F. Finite elastic strain of cubic crystals. *Phys. Rev.* **71**, 809–824 (1947).
37. Sakakibara, H. et al. Theoretical analysis on the possibility of superconductivity in the trilayer Ruddlesden-Popper nickelate $La_4Ni_3O_{10}$ under pressure and its experimental examination: comparison with $La_3Ni_2O_7$. *Phys. Rev. B* **109**, 144511 (2024).
38. Xu, M. et al. Pressure-dependent "Insulator–Metal–Insulator" behavior in Sr-doped $La_3Ni_2O_7$. *Adv. Electron. Mater.* **10**, 2400078 (2024).
39. Cheng, J.-G. et al. Integrated-fin gasket for palm cubic-anvil high pressure apparatus. *Rev. Sci. Instrum.* **85**, 093907 (2014).
40. Garlea, V. O. et al. The high-resolution powder diffractometer at the high flux isotope reactor. *Appl. Phys. A.* **99**, 531–535 (2010).
41. Calder, S. et al. A suite-level review of the neutron powder diffraction instruments at Oak Ridge National Laboratory. *Rev. Sci. Instrum.* **89**, 092701 (2018).
42. Rodríguez-Carvajal, J. Recent advances in magnetic structure determination by neutron powder diffraction. *Phys. B Condens. Matter* **192**, 55–69 (1993).
43. Toby, B. H. & Von Dreele, R. B. GSAS-II: the genesis of a modern open-source all purpose crystallography software package. *J. Appl. Crystallogr.* **46**, 544–549 (2013).
44. Kresse, G. & Furthmüller, J. Efficiency of ab-initio total energy calculations for metals and semiconductors using a plane-wave basis set. *Comput. Mater. Sci.* **6**, 15–50 (1996).
45. Kresse, G. & Joubert, D. From ultrasoft pseudopotentials to the projector augmented-wave method. *Phys. Rev. B* **59**, 1758–1775 (1999).
46. Perdew, J. P., Burke, K. & Ernzerhof, M. Generalized gradient approximation made simple. *Phys. Rev. Lett.* **77**, 3865–3868 (1996).
47. Dudarev, S. L., Botton, G. A., Savrasov, S. Y., Humphreys, C. J. & Sutton, A. P. Electron-energy-loss spectra and the structural stability of nickel oxide: an LSDA+U study. *Phys. Rev. B* **57**, 1505–1509 (1998).

Acknowledgements

This work is supported by the National Key Research and Development Program of China (2023YFA1406100, 2021YFA1400200), the National Natural Science Foundation of China (12025408, 12404179, 11921004, U23A6003, 12304030, 12174424), the Strategic Priority Research Program of CAS (XDB33000000), the Postdoctoral Fellowship Program of China Postdoctoral Science Foundation (GZB20230828, GZB20230674), the China Postdoctoral Science Foundation (2023M743740), CAS PIFI program (2024PG0003), and CAS Project for Young Scientists in Basic Research (2022YSBR-047). J.Q.Y. was supported by the U.S. Department of Energy, Office of Science, Basic Energy Sciences, Division of Materials Sciences and Engineering. High-pressure synchrotron X-ray measurements were performed at the BL15U1 station and User Experiment Assist System of the Shanghai Synchrotron Radiation Facility (SSRF), which is supported by the Chinese Academy of Sciences. This research used resources at the High Flux Isotope Reactor, a U.S. DOE Office of Science User Facility operated by the Oak Ridge National Laboratory.

Author contributions

J.G.C. designed the project. G.W. and N.N.W. synthesized the materials and characterized their structure via XRD; G.W., N.N.W., L.F.S., J.H. and L.M. measured the HP-SXRD and analyzed the data with the support of J.P.S., B.S.W. and L.L.Z.; S.C. and J.Q.Y. measured and analyzed the NPD data; T.L.L. performed the DFT structure calculations with the support of S.M. and M.L.; J.G.C., N.N.W. and G.W. wrote the paper with inputs from all coauthors.

Competing interests

The authors declare no competing interests.

Additional information

Supplementary information The online version contains supplementary material available at https://doi.org/10.1038/s41535-024-00721-8.

Correspondence and requests for materials should be addressed to Ningning Wang, Miao Liu or Jinguang Cheng.